International Journal on Advanced Science Engineering Information Technology

Vol.11 (2021) No. 3
ISSN: 2088-5334

Development of Chemiluminescence Resonance Test System Using SiPM Front-end ASIC to Detect Na and K Ions in Urine

Hojong Chang[a,*], KyungDon Choi[b], Byunghun Han[a], Hyunduk Kim[c], Jaeho Ko[d], Gyuseong Cho[e]

[a]*Institute for Information Technology Convergence, KAIST, 291 Daehak-ro, Yuseong-gu, Daejeon, 34141, Republic of Korea*
[b]*UCSF Helen Diller Family Comprehensive Cancer Center, 1600 Divisadero Street, San Francisco, CA 94143-1708, USA*
[c]*IRIS Co., Ltd., A609, 193 Munji-ro, Yuseong-gu, Daejeon, 34051, Republic of Korea*
[d]*SungsanENG Corp., 142-19 Sanho-daero, Gumi, Gyeongsangbuk-do, 39377, Republic of Korea*
[e]*Department of Nuclear & Quantum Engineering, KAIST, 291 Daehak-ro, Yuseong-gu, Daejeon, 34141, Republic of Korea*
Corresponding author: [*]hojoungc@kaist.ac.kr

***Abstract*— The importance of measure and control dietary salinity arises to prevent and control the disease. There are several methods to measure the dietary salinities from blood or urine. The blood test is an accurate but inconvenient method because patients need to be at hospitals and wait for a longer time. Urine can be collected at home, and the test is more convenient. A 24-hour urine test is more accurate than random urine (RU) may cause more human errors. For this reason, testing RU accuracy for application will increase the convenience of patients. A SiPM sensor system to measure Guanine-based chemiluminescence resonance test light was developed. An ASIC system was developed and packaged to a chip. A test board for the packaged chip was developed. In parallel, the layout of an ASIC chip was assembled with SiPM and tested in the dark chamber to understand the functionality. The ASIC chip was tested in various frequencies with the test board. At the target frequency, the ASIC chip achieved 870 gain, which is exceeding the goal of 100. The SiPM system was measured with an oscilloscope, and the output signal was as expected. The performance test was done at a very high frequency (100MHz) and achieved 80.5% detection compared to the original light source signal. The ASIC chip development was successful, and SiPM matched the specification of the target operation.**

***Keywords*— SiPM; RU; ASIC; Sodium; Potassium; Photon.**

Manuscript received 20 Aug. 2020; revised 10 Jan. 2021; accepted 24 Feb. 2021. Date of publication 30 Jun. 2021.

I. INTRODUCTION

It is easy to think about many diseases caused by dietary salinity, such as hypertension, stroke, coronary artery disease, cardiovascular disease, kidney disease, stomach cancer, etc. Potassium and sodium are necessary dietary salinities that may cause several diseases when abundance [1]-[11]. For this reason, both healthy and diseased people need to measure the amount of potassium and sodium to prevent and relieve disease. Respectively [3], [4], [12], [13]. World Health Organizations (WHO) recommend not eating sodium more than 2g/day or 88mmol/day [14]. Urine test is one of the most widely used test methods for dietary sodium and potassium alternate the blood test [15], [16]. There are two types of urine tests for sodium and potassium test: a 24-hour urine test and random urine (RU) test. A 24-hour urine test is more accurate than a RU test because sodium and potassium in urine vary with the dietary condition. However, there are also some limitations to the 24-hour urine test. For example, patients forgot to collect urine at the proper time, and the price for the test is higher than RU.

In many cases, RU test accuracy matches good agreement [17]-[20]. Thus, developing a cheap and accurate RU test method would benefit a large population who may need a urine test. Several devices can measure sodium and potassium in the blood. Siemens ADVIA 2400 is a big-size device confirmed to be used in hospitals, MEDICA EasyLyte Plus is a medium-size tester, and ABBOTT i-STAT is a portable device with a one-time use kit. Most of the small urine test devices are colorimetric type [21]-[23]. Those devices detect leukocyte, nitrite, pH, protein, sugar, ketone, urobilinogen, bilirubin, red blood cell, etc. However, current devices in the market cannot measure sodium and potassium without diluting the urine. It is hard to find any portable device that measures both salinities directly. If sodium and potassium measurement is required, it is necessary to send the sample to large hospitals and wait more than 3 hours to a few days. One of the popular methods for medical science is high-pressure

liquid chromatography (HPLC) and electrophoresis [24], [25]. Those methods require high price devices, and foreign substances may cause malfunctioning. Antibodies are used to overcome the disadvantages mentioned above. Radioactive materials were attached to antibodies for accurate detection, but control of radioactive materials and safety issue remains. Absorbance, fluorescence, and chemiluminescence were developed to overcome the radioactive antibody limitation. In this research, the Guanine-based chemiluminescence resonance test was used to measure the amount of sodium and potassium directly [26]-[28]. Fig. 1 shows the reaction of Guanine-TMPG to how the light is emitted.

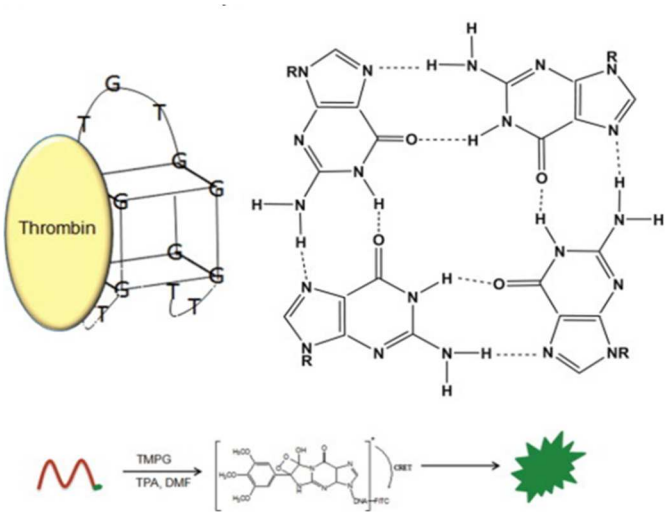

Fig. 1 A chemical mechanism of Guanine-TMPG reaction [29].

Traditionally, photon multiplier tube (PMT) has been used for various fields such as low light level spectroscopy, confocal microscopy, Raman spectroscopy, fluorescence spectroscopy, nuclear and particle physics, astronomy, medical diagnostics, including blood tests, medical imaging, motion picture film scanning, and radar jamming. The photo-electric effect, well known for Albert Einstein's experiment to show the electron is a particle rather than a wave, is the principle of PMT. When a photon comes to the photocathode in front of PMT and emits a primary electron, the primary electron hits series of dynodes in high voltage to amplify the numbers of electrons. PMT is a very accurate and reliable device for photon detection. However, PMT has some natural limitations. As PMT is a vacuum tube, it is hard to make a small PMT, and the cost increases with the decreases in its size. The operating voltage is about a few thousands volt to amplify the electrons, so that the background electronics are enormous and expensive. Alternatively, a silicon photon multiplier (SiPM) was developed to detect photons. SiPM is a semiconductor-based detector that can overcome the limitation of PMT mentioned above. SiPM is easy to downsize, and the cost is reasonable. The operating voltage is about a maximum of 100V, and it is much lower than the PMT. A photon detection system for alternative sodium and potassium measurement method from RU is presented in this research. A photon generator was developed to test the system, and the result is given in this research.

II. Material and Methods

A. SiPM

SiPMs from different manufacturers such as Hamamatsu photonics, SeneL, and Ketek is considered in this research. The essential characteristics of other manufacturers SiPM is the breakdown voltage (V_{BR}) and recommended operating voltage (V_{OP}). The V_{BR} and V_{OP} for considered SiPMs are given in Table 1.

TABLE I
SIPM V_{BR} AND V_{OP}

Manufacture	Models	V_{BR} [V]	V_{OP} [V]
Hamamatsu Photonics	S13360-1325CS	53±5	V_{BR} + 5
	S13360-1350CS	53±5	V_{BR} + 5
	S13360-1375CS	53±5	V_{BR} + 5
SeneL	C-Serise	24.2 to 24.7	V_{BR} + 1 to 5
Ketek	PM1125-WB	Typ. 25.5	V_{BR} + 2 to 5

Additionally, the gain is another factor to be considered. The higher increase that SiPM has, the better signal detection is expected. However, the gain can be controlled by adjusting the voltage. As V_{OP} for Hamamatsu Photonics SiPMs requires ~ 60V and the others are 30V, the voltage supply system was considered to provide variable voltage.

B. System Layout

The signal from SiPM cannot be read and understood directly. For this reason, the project dedicated Application Specific Integrated Circuit (ASIC) attached with SiPM was developed. The maximum size of the full system was limited to 225mm^2 square to match the downsizing goal. The block diagram for Front-end ASIC is shown in Fig. 2.

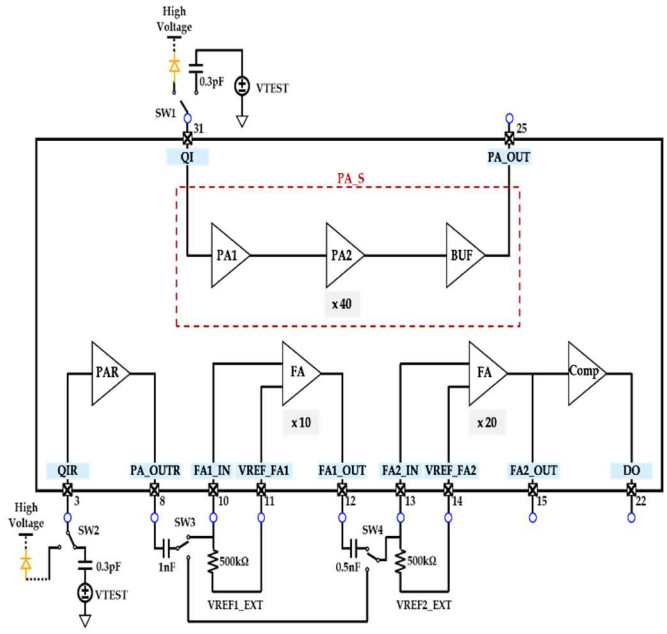

Fig. 2 Front-end ASIC block diagram for main and subcircuit. The main and subcircuits are in the lower and upper part, respectively.

The main circuit is the operating system, and the subcircuit is used only for measurement. The main circuit is designed to control 2 step amplifiers to obtain proper gain from the signal.

This front-end ASIC was packaged with QFN32. The layout, bare die, and packaged chi are shown in Fig. 3.

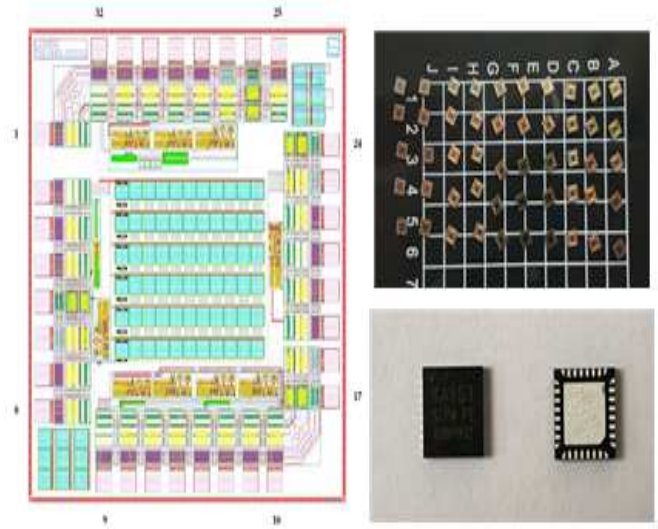

Fig. 3 The layout, bare die, and packaged chip. The left side is the layout, the upper right is bare die, and the bottom right is a packaged chip.

A test board to test ASIC was developed as well. The test board can monitor all signals going in and processed from the ASIC chip. The test board is shown in Fig. 4.

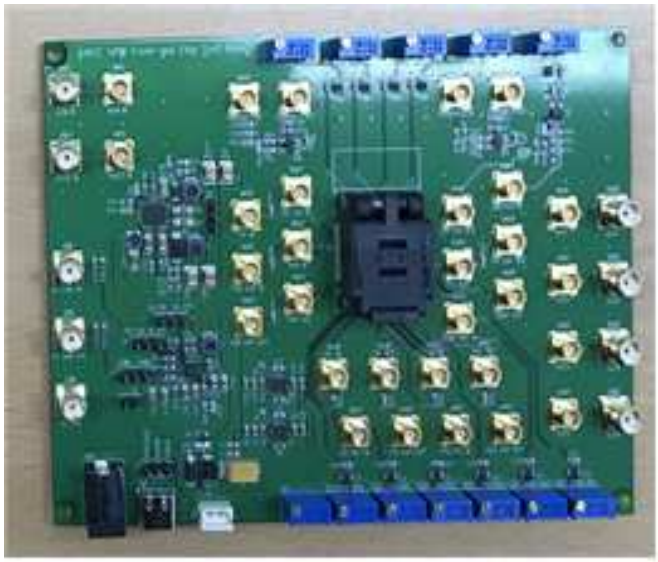

Fig. 4 The developed ASIC circuit. The ASIC will be located at the centre of the board, and all the signals can be connected to an oscilloscope.

In the meantime, SiPM was tested independently from the ASIC chip to obtain SiPM data for further use. For this reason, a temporary amplification board sharing the layout in Fig. 3 was developed independently and attached to SiPM for the layout test. In Fig .5, the test board sharing the layout was attached to SiPM aligned with the photon generator, which will be explained in the following. Before manufacturing the chip, the simulation was performed to understand if the design is correct with the Cadence tool. The simulation predicts the results in ideal cases that simulation was performed in the higher frequency (20MHz) than the target frequency (12MHz).

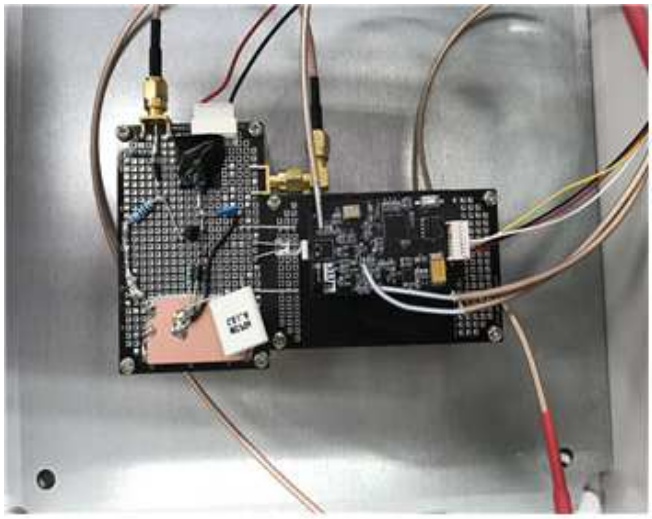

Fig. 5 A SiPM with test board sharing the ASIC layout (right side) and the photon generator (left side) is given.

C. *Photon generator*

It may be enough to build a photon generator matching for the target frequency specification (12MHz). However, one of the experiments is to understand the limitations of the SiPM system. For this reason, the photon generator was designed to be operated at a higher frequency (100MHz). Thus, the LED signal should decay much faster than SiPM or amplified signal. A fast pulse design was considered to achieve the specification of a photon generator. The layout of the photon generator circuit is shown in Fig. 6.

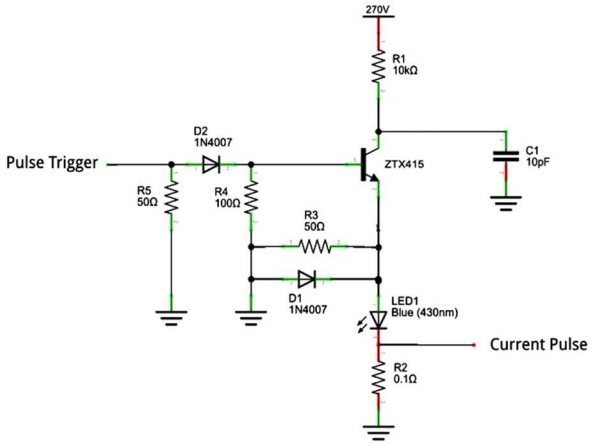

Fig. 6 The layout of the photon generator is shown. [30]

The spike is ~0.5V with a decay time of less than 10ns. The photon generator can stably provide photons at 100MHz, which is highly exceeding the target frequency.

D. *Experiment design*

The signal coming from the SiPM is shallow, and the minimum signal power that the function generator could generate is 20mVpp. Thus, a capacitor (0.3pF) was implemented at the front to decrease the power coming from the function generator up to 0.2mVpp when the function generator output power is 40mVpp. However, this work is affected by the oscilloscope probe so that the capacitor input and output were measured independently, and this data was used for the calibration of the results. The expected operating frequency is 12MHz, so that the test was performed with 1, 4,

8, 10, 11, 12, 13, 14MHz. The gain was measured with the same operating frequency mentioned above. The minimum requirement for gain is 100, that at least the gain needs to be higher at near 12MHz operating frequency. Gain is defined as total output/input. The SiPM testing system is measuring the numbers of photon emission events coming from the photon generator. SiPM is aligned to the photon generator not to miss the signal. Photon events are generated with a function generator that the frequency of events is coming in an exact time interval. As the signals are generated with a function generator, the ratio between SiPM detection and function generator is measured. The measurement was performed in a dark chamber in Fig. 7.

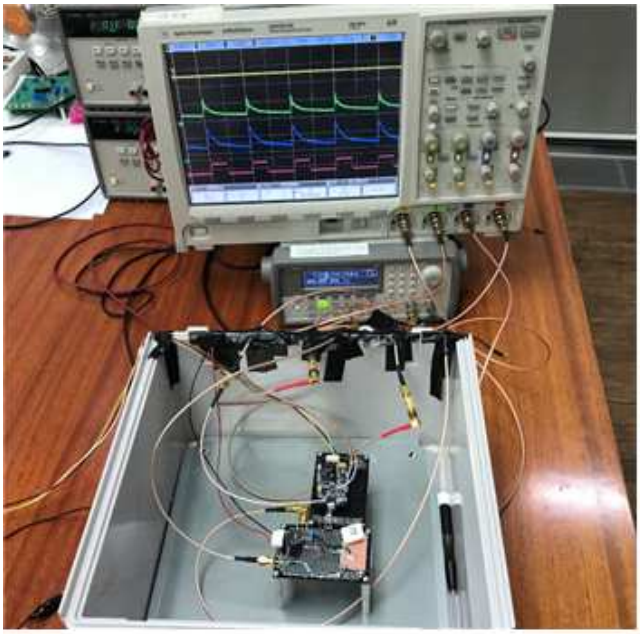

Fig. 7 Test environment in the dark chamber. The cable output line is also sealed with black insulation taping to prevent light coming from the outside.

The home-made dark chamber is designed to perform photon detection for various experimental systems, including radiation experiments. Thus, the dark chamber should not leak light, or the background noise would exceed the proper measurement signals. For this reason, the cable exiting area is also sealed with black insulation tape. It was tested to have a shallow background signal compared to the SiPM.

III. Results and Discussion

A. Front-end ASIC Test Board

The simulation results are shown in Fig. 8. 2MHz and 20MHz results are given together. Both of the simulation inputs are in an ideal condition so that the results are very stable. In Table 2 and Fig. 9, selected operating frequency input outputs from each amplifier are shown.

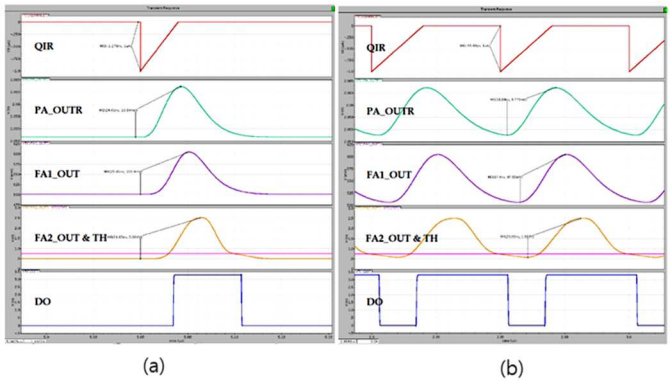

Fig. 8 The simulation results for the front-end ASIC chip. (a) and (b) are 2MHz and 20MHz simulation results, respectively. From the top, ASIC input signal, amplified signals, and data output is given.

TABLE II
INPUT AND CAPACITOR OUT VOLTAGE TABLE FOR EACH EXPERIMENTAL OPERATING FREQUENCIES.

Operating Frequency (MHz)	Input (mVpp)	Capacitor out (mVpp)
1	40.0	0.25
4	39.3	0.24
8	36.4	0.20
10	35.0	0.26
11	34.2	0.24
12	33.5	0.23
13	32.9	0.21
14	32.4	0.20

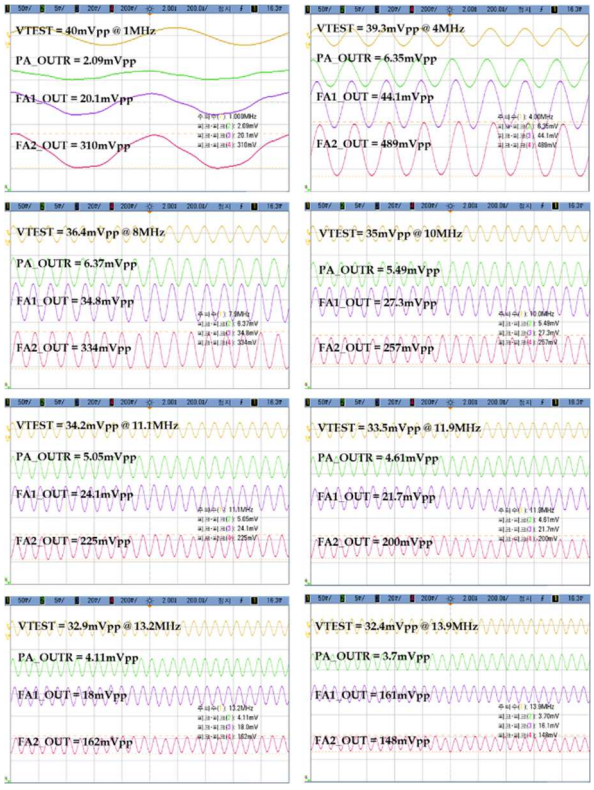

Fig. 9 From the top of each independent images, function generator signal, input, the output from the first amplifier and output from the second amplifier is given. (a), (b), (c). (d). (e), (f), (g) and (h) are 1, 4, 8, 10, 11, 12, 13 and 14 MHz operating frequency results.

The decrease of input power from 40mVpp is not linear between 1 and 4MHz. However, the voltage drop is linear from 4MHz to 14MHz. In the meantime, the output voltage is not linear at all. The output voltage decreases from 0.25mVpp to 0.2mVpp for 1 to 8MHz. Then the output increases up to 0.26mVpp and decreases to 0.2mVpp continuously. At the 12MHz frequency, which is the targeting frequency, the output was 0.23mVpp. The total gain for each frequency is shown in Table 3.

TABLE III
INPUT, FINAL OUTPUT AND GAIN TABLE FOR EACH EXPERIMENTAL OPERATING FREQUENCIES.

Operating Frequency (MHz)	Input (mVpp)	Output (mVpp)	Gain
1	0.25	310	1240
4	0.24	489	2038
8	0.20	334	1670
10	0.26	257	1285
11	0.24	225	938
12	0.23	200	870
13	0.21	162	711
14	0.20	148	740

Gain is increasing from 1MHz to 4MHz and decreases up to 14MHz. The maximum gain at 4MHz is 2038, which means that the signal was amplified 20 times more than the original signal. There exists a weak correlation between the raw voltage input and the gain. At the targeting frequency, the gain is 870.

B. Photon count in the dark chamber

Four signals, LED signal from the photon generator, raw SiPM output, amplification out and COMP out, were measured to understand the behaviour of signals coming from the SiPM. Single signal phase read with an oscilloscope is shown in Fig. 10.

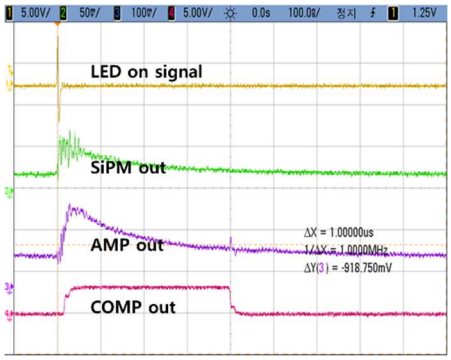

Fig. 10 Various signals read with an oscilloscope. The LED signal from the photon generator, SiPM raw signal, amplified signal, and COMP out are shown from the top.

The signal on the top is the LED signal generated with a function generator. The LED signal activated in a relatively short time compared to other signals. The second signal is a raw SiPM signal. Raw SiPM signal is activated just after the LED signal is initiated. Then the signal starts decaying from its maximum signal. Then the amplified signal reacts a few moments after the SiPM signal was generated. This result is due to the required processing time in the amplification circuit. There exists a small noise for the amplified signal where the comparator signal is deactivated. The comparator signal shows the area where the amplified signal is over the threshold to distinguish signals.

Sets of signals read with an oscilloscope is shown in Fig. 11. As it is mentioned above, the decay time for the LED signal is much shorter than the operating frequency. For this reason, LED signal generation can be considered as a point source. Then the SiPM raw signal and amplified signals show a very similar decay. All the amplified signals have noise where the comparator signals are fade out. As a result, comparator signals show the area where the valid amplified signals are located.

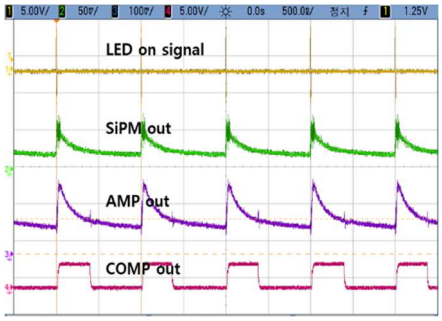

Fig. 11 Series of signals read with an oscilloscope. The LED signal from the photon generator, SiPM raw signal, amplified signal, and COMP out are shown from the top.

In total, 80.5% of signals were measured at about 100MHz with the board in the dark chamber, with respect to the LED and function generator signal counts.

C. Discussion

The ASIC chip test was performed with the chip test board. Considering the gain and final output, the best operating frequency for the ASIC is 4MHz. The gain was decreased at the target frequency (12MHz). However, the expected gain at the target frequency is 100, and the gain was 870. The result exceeds the expectation, and the ASIC chip design and manufacture seem to be satisfactory. As a result, the ASIC chip functions were tested, and the ASIC chip is properly working as expected. The simulation was performed at a higher frequency than the target frequency because the real operating frequency for the chip is lower than the simulated frequency. The simulation result shows the higher gain against the ASIC test. The result of mismatch is coming from the simulation setting. The simulation predicted the gain with the best condition, which is impossible to match in the real world. Thus, it is nice to consider the real circumstances when performing the simulation and consider that the experimental result will be worse than the simulation result.

The photon generator decay time is much fast than that of SiPM and amplification circuits. This result implies that the photon generator can be considered as a single event. SiPM and amplification circuit decay time are much longer than the LED signal. However, putting the proper threshold after the amplification circuit can distinguish between two short-term events. The amplified signal has a small noise when the amplified signal undergoes the threshold that the comparator signal is deactivated. The noise is relatively lower than the peak of itself and decays quickly so that the noise would not

affect the other signal. The SiPM signal detection was about 80.5% at 100MHz. As the target frequency is much lower than 100MHz, we can expect that almost all the signals coming from the urine chemical light will be read and recorded with the system. After the ASIC chip is confirmed, the SiPM board will be replaced with ASIC chip. Then the board itself will be downsized and easier to be assembled.

IV. Conclusion

We developed an ASIC chip, test board, photon generator, and test amplification circuit for the urine chemical luminescence. The ASIC chip passed the test with its test board. SiPM was tested with the same layout of the developed ASIC chip and showed satisfactory results. The fully integrated board will be manufactured for the final product. The detection system developed in this research is minimal and fast reacting. Thus, the final product of this research is planned to be used as a ubiquitous health point of care testing for healthy and diseased users. Results of point-of-care testing tend to be discarded. Using a Mashup-Platform, Device-Platform as an IoT platform comparison with subsequent results and historical data will easily.

Acknowledgment

This research is funded by the National Research Foundation of Korea (NRF-2015M3A7B7045525) and the KI institution-specific project of 2020 KAIST's research project(N11200158).

References

[1] Schmidt, C. W. (2017). Another side of a low-salt diet: Reductions in the salinity of drinking water may lower blood pressure. Environmental Health Perspectives. https://doi.org/10.1289/EHP2099

[2] Biggers, A., & Felman, A. (2019). Medical-News-Today_High blood pressure: What is high, symptoms, causes, and more.

[3] Houston, M. C. (2011). The importance of potassium in managing hypertension. Current Hypertension Reports.

[4] Grillo, A., Salvi, L., Coruzzi, P., Salvi, P., & Parati, G. (2019). Sodium intake and hypertension. Nutrients.

[5] A. Stallings, M. Harrison, & M. Oria (2019). Dietary Reference Intakes for Sodium and Potassium. National Academies Press.

[6] Shlezinger, M., Amitai, Y., Akriv, A., Gabay, H., Shechter, M., & Leventer-Roberts, M. (2018). Association between exposure to desalinated sea water and ischemic heart disease, diabetes mellitus and colorectal cancer; A population-based study in Israel. Environmental Research, 166, 620–627. https://doi.org/10.1016/j.envres.2018.06.053

[7] Naser, A. M., Rahman, M., Unicomb, L., Doza, S., Gazi, M. S., Alam, G. R., Karim, M. R., Uddin, M. N., Khan, G. K., Ahmed, K. M., Shamsudduha, M., Anand, S., Narayan, K. M. V, Chang, H. H., Luby, S. P., Gribble, M. O., & Clasen, T. F. (2019). Drinking Water Salinity, Urinary Macro-Mineral Excretions, and Blood Pressure in the Southwest Coastal Population of Bangladesh. Journal of the American Heart Association, 8(9).

[8] Gianfredi, V., Bragazzi, N. L., Nucci, D., Villarini, M., & Moretti, M. (2017). Cardiovascular diseases and hard drinking waters: Implications from a systematic review with meta-analysis of case-control studies. Journal of Water and Health, 15(1), 31–40.

[9] Koren, G., Shlezinger, M., Katz, R., Shalev, V., & Amitai, Y. (2017). Seawater desalination and serum magnesium concentrations in Israel. Journal of Water and Health, 15(2), 296–299.

[10] Wu, J., Xun, P., Tang, Q., Cai, W., & He, K. (2017). Circulating magnesium levels and incidence of coronary heart diseases, hypertension, and type 2 diabetes mellitus: A meta-analysis of prospective cohort studies. Nutrition Journal, 16(1).

[11] O'Connor, L. E., Hu, E. A., Steffen, L. M., Selvin, E., & Rebholz, C. M. (2020). Adherence to a Mediterranean style eating pattern and risk of diabetes in a US prospective cohort study. Nutrition and Diabetes, 10(1). https://doi.org/10.1038/s41387-020-0113-x

[12] Seko, C., Odani, K., Wada, S., Yoshii, K., Segawa, H., Kitaoka, K., Masumoto, T., & Higashi, A. (2020). Characteristic dietary habits associated with high values of estimated 24-hours urinary sodium excretion and sodium-to-potassium ratio assessed by age group among the residents of a rural town in Japan. Clinical and Experimental Hypertension, 42(5), 449–459.

[13] Hojong, C., Byunghun, H., Gyuseong, C., & Hyunduk, K. (2018). A Study on the Measurement of Aptamer in Urine Using SiPM. Journal of Advanced Research in Dynamical and Control Systems, 11-Special Issue, 1208–1210.

[14] Kieneker, L. M., Gansevoort, R. T., Mukamal, K. J., De Boer, R. A., Navis, G., Bakker, S. J. L., & Joosten, M. M. (2014). Urinary potassium excretion and risk of developing hypertension: The prevention of renal and vascular end-stage disease study. Hypertension.

[15] Jędrusik, P., Symonides, B., & Gaciong, Z. (2019). Performance of 24-hour urinary creatinine excretion-estimating equations in relation to measured 24-hour urinary creatinine excretion in hospitalized hypertensive patients. Scientific Reports, 9(1).

[16] Jędrusik, P., Symonides, B., & Gaciong, Z. (2018). Comparison of three formulas to estimate 24-hour urinary sodium and potassium excretion in patients hospitalized in a hypertension unit. Journal of the American Society of Hypertension, 12(6), 457–469.

[17] Koo, H., Lee, S.-G., & Kim, J.-H. (2015). Evaluation of random urine sodium and potassium compensated by creatinine as possible alternative markers for 24 hours urinary sodium and potassium excretion. Annals of Laboratory Medicine, 35(2), 238–241.

[18] Park JE, Lee CH, Kim BS, Shin IH. (2010). Diagnostic usefulness of the random urine Na/K ratio in cirrhotic patients with ascites: a pilot study. Korean J Hepatol.

[19] Jędrusik, P., Symonides, B., Wojciechowska, E., Gryglas, A., & Gaciong, Z. (2017). Diagnostic value of potassium level in a spot urine sample as an index of 24-hour urinary potassium excretion in unselected patients hospitalized in a hypertension unit. PLoS ONE

[20] Lin, C., Piao, X., Pan, Q., Li, J., Shan, Z., & Teng, W. (2017). Spot urine potassium-creatinine ratio is a good alternative marker for 24-hour urine potassium in differential diagnosis of Hypokalemia. Medical Science Technology, 58, 137–144.

[21] Ye, J., Li, N., Lu, Y., Cheng, J., & Xu, Y. (2017). A portable urine analyzer based on colorimetric detection. Analytical Methods. https://doi.org/10.1039/c7ay00780a

[22] Yang, R., Cheng, W., Chen, X., Qian, Q., Zhang, Q., Pan, Y., … Miao, P. (2018). Color Space Transformation-Based Smartphone Algorithm for Colorimetric Urinalysis. ACS Omega. https://doi.org/10.1021/acsomega.8b01270

[23] He, Y., Dong, K., Hu, Y., & Dong, T. (2017). Colorimetric recognition for urinalysis dipsticks based on quadratic discriminant analysis. Proceedings of the Annual International Conference of the IEEE Engineering in Medicine and Biology Society, EMBS.

[24] Waters. (2016). How does high performance liquid chromatography work? : Waters. https://doi.org/10.1162/PAJJ_a_00279

[25] Oka, K., & Furusawa, K. (2018). Electrophoresis. In Electrical Phenomena at Interfaces: Fundamentals Measurements, and Applications, Second Edition, Revised and Expanded.

[26] Dong, J., Lian, J., Jin, Y., & Li, B. (2017). Guanine-based chemiluminescence resonance energy transfer biosensing platform for the specific assay of uracil-DNA glycosylase activity. Analytical Methods. https://doi.org/10.1039/c6ay02964g

[27] Chen, Z., Guo, J., Zhang, S., & Chen, L. (2013). A one-step electrochemical sensor for rapid detection of potassium ion based on structure-switching aptamer. Sensors and Actuators, B: Chemical.

[28] Shi, C., Gu, H., & Ma, C. (2010). An aptamer-based fluorescent biosensor for potassium ion detection using a pyrene-labeled molecular beacon. Analytical Biochemistry.

[29] Cho, S., Park, L., Chong, R., Kim, Y. T., & Lee, J. H. (2014). Rapid and simple G-quadruplex DNA aptasensor with guanine chemiluminescence detection. Biosensors and Bioelectronics.

[30] (2018) Fast LED Light Pulser & SiPM. http://physicsopenlab.org/2018/12/02/fast-led-light-pulser-sipm/